Dissociative-electron-attachment dynamics near the 8-eV Feshbach resonance of CO_2

A. Moradmand,[1] D. S. Slaughter,[2] A. L. Landers,[1] and M. Fogle[1]
[1]*Physics Department, Auburn University, Auburn, Alabama 36849-5311, USA*
[2]*Lawrence Berkeley National Laboratory, Chemical Sciences, Berkeley, California 94720, USA*
(Received 17 July 2013; published 30 August 2013)

We present experimental results for dissociative electron attachment to carbon dioxide near the 8-eV Feshbach resonance. In particular, the dissociation channel leading to O^- production has been investigated with a momentum imaging technique that utilizes a supersonic gas jet to form a low-temperature, confined molecular target. Angular fragmentation and kinetic energy release distributions are compared to recent results by Slaughter *et al*. [J. Phys. B **44**, 205203 (2012)] and Wu *et al*. [Phys. Rev. A **85**, 052709 (2012)] using similar techniques. We show that careful attention to weighting of the O^- fragmentation momentum space is required to interpret the kinetic energy release observations and that there is no appreciable change in the angular distribution of O^- fragments at different energies around the resonance peak, as previously reported by Wu *et al*. The present O^- momentum distribution and kinetic energy release differ from previous results and provide alternative guidance for the theoretical consideration of potential energy surface dynamics that takes place during attachment.

DOI: 10.1103/PhysRevA.88.022711 PACS number(s): 34.80.Ht

I. INTRODUCTION

Dissociative electron attachment (DEA) is a dominant dissociation mechanism leading to the production of stable anions from electrons at energies below 10 eV. Extant literature on this mechanism in CO_2 provides information on cross sections and ion energy as well as angle specific dissociation utilizing electron beam monochromators and mass analyzers [1–8], while newer experimental techniques have allowed three-dimensional (3D) imaging of the dissociation dynamics [9–11]. Dissociative attachment resonances for this system are well known, with a shape resonance appearing near 4 eV and a Feshbach resonance near 8 eV. The resonance at 8 eV was earlier attributed to a $^2\Sigma_g^+$ state [7,12], but later researchers determined that a Feshbach resonance of $^2\Pi_g$ character is the likely resonant state [5,8,13]. Further, Slaughter *et al*. [14] determined that a conical intersection exists between the $^2\Pi_g$ state of the transient anion at 8 eV and the $^2\Pi_u$ state at 4 eV. Nuclear dynamics and nonadiabatic coupling between these two anion potential energy surfaces determines the final states of the dissociation.

Angle- and energy-resolved imaging on DEA to carbon dioxide, particularly at the 8-eV Feshbach resonance, have revealed an anisotropic angular distribution for the resulting O^- anion with a minimum located in the forward incoming electron direction. Additionally, a near-zero energy contribution was observed in the momentum distribution when confined to a thin slicing-plane containing the incoming electron's momentum vector [7,8,14,15]. Our work shows that the contribution from this near-zero energy contribution is exaggerated by the treatment of the data. Also, recent attempts to explain the mechanism of dissociative attachment via the Renner-Teller effect, by fitting the measured angular distributions with spherical harmonics, are belied by observations of a clear nonaxial recoil effect observed in the O^- angular fragment distribution.

II. EXPERIMENT

The details of the apparatus have been discussed in a previous publication and will only be outlined here [16]. Figure 1 illustrates the crossed-beam geometry of the momentum imaging spectrometer used in our study of DEA to CO_2. A skimmed, supersonic gas jet target is crossed with a pulsed electron beam in the COLTRIMS-type spectrometer to produce the electron-molecule interactions [17]. The gas jet is dumped into a catcher region where the excess gas is pumped away. The target confinement (2 mm) and low temperature (20 K) of the supersonic gas jet are a significant advantage over effusive targets. Effusive targets almost always have to contend with the significant spacial extent of the interaction region, such as by means of electrostatic lensing and adjusting the magnetic collimating field for the electron beam. It has also been shown that vibrational excited states in the target can lead to different DEA mechanisms and resultant dynamics.

A pulsed electron beam with a 100 ns full width at half maximum (FWHM) is created with a commercial electron gun (Kimball Physics ELG-2) with energy resolution of 1.0 eV FWHM. The electron beam has an estimated spot size of $\sim$1 mm at the interaction region. The electron beam, and subsequent ion extraction field, are pulsed at a repetition rate of $\sim$40 kHz. The two beams intersect at the interaction point centered in the spectrometer where a uniform electric field extracts anions onto a time- and position-sensitive detector via a field-free drift region. While electrons are in the interaction region, the spectrometer is kept field-free and the resulting dissociation anion fragments are allowed to expand for 0.5 μs. The pulsed extraction electric field is then turned on by pulsing a gridded repeller plate to -50 V for 10 μs, pushing anions through this region into a field-free drift region where dissociation fragments are allowed to separate further before impacting a microchannel plate detector with a delay line anode. Timing signals received from the microchannel plates, with respect to an electron beam pulse, provide time-of-flight information for the anions, while the delay line anode allows position determination through the measurement of pulse timing differences from opposite ends of anode wire pairs. A constant $\sim$30 G magnetic field collimates the electron beam but has negligible effect on the ions flight trajectories.

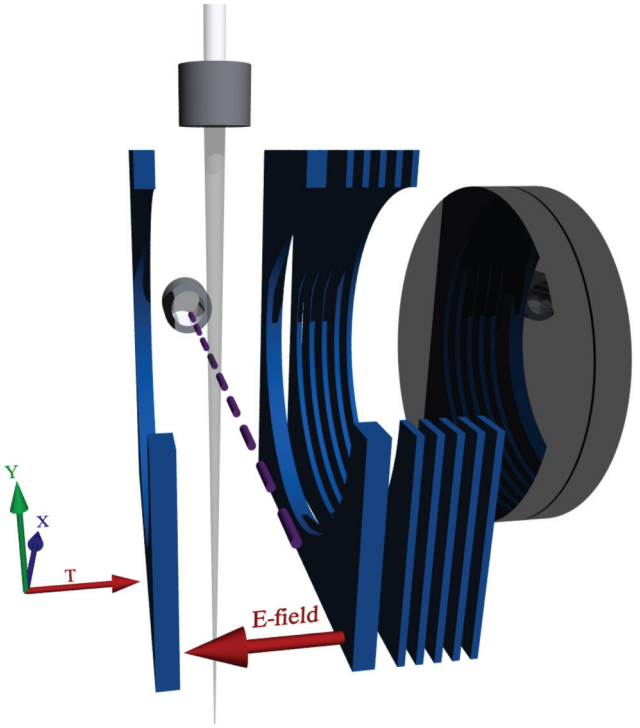

FIG. 1. (Color online) Cutaway illustration of the DEA imaging apparatus. A pulsed beam of electrons (along the X axis) is crossed with a supersonic gas jet (long the Y axis). Ionic dissociation fragments resulting from the interaction are subsequently extracted to the detector (along the T axis) with a pulsed electric field in between electron bunches.

Event-mode data are acquired by the proprietary COBOLDPC [18] data acquisition program and analysis of the data is performed in the ROOT [19] analysis framework software package. The position and timing information of the anions is used to calculate the initial post-interaction momentum in three dimensions. These data are then used to determine the ion kinetic energy and ion fragment angular distribution relative to the electron beam axis.

III. RESULTS AND DISCUSSION

The momentum-space density plots in Fig. 2 show an anisotropic distribution with a clear minimum in the forward incoming electron direction and peaks in the angular distribution appearing at $\pm 50^\circ$ and $\pm 130^\circ$, with respect to the initial electron direction. In Fig. 2, the X direction is defined by the initial electron momentum vector and the T direction points toward the detector, so that the jet direction is out of the image plane. Figure 2(a) shows the momentum sphere sliced through the center by constraining the data to within ± 5.4 a.u. momentum in the Y direction, while Fig. 2(b) is the same data weighted to account for the changing solid angle by constraining the elevation angle, $\phi = \tan^{-1}(P_Y/\sqrt{P_X^2 + P_T^2})$, of the momentum to within $\pm 5^\circ$. This effectively forms a wedge whose vertex is at the origin of the momentum space and is revolved around the selected slicing plane. This constraining angle of the wedge is chosen to coincide with the estimated momentum resolution of the experiment. As the radius increases, the angle of acceptance is held constant so that fragments of differing energy are treated equally.

The center, low-energy feature is clearly visible in the unweighted slice shown in Fig. 2(a) but not in the weighted data shown in Fig. 2(b). This is because a flat slice of the data exaggerates the contribution of the lower energy ions against those of higher energy. Consider the extreme case of O^- produced in a pointlike volume with a bimodal kinetic energy distribution, with one component having kinetic energy of nearly 0 eV and another component with equal yield having kinetic energy of exactly 0.6 eV. The 3D ion momentum image would appear as a dot surrounded by a thin spherical shell that we shall consider to be uniform over both azimuthal and

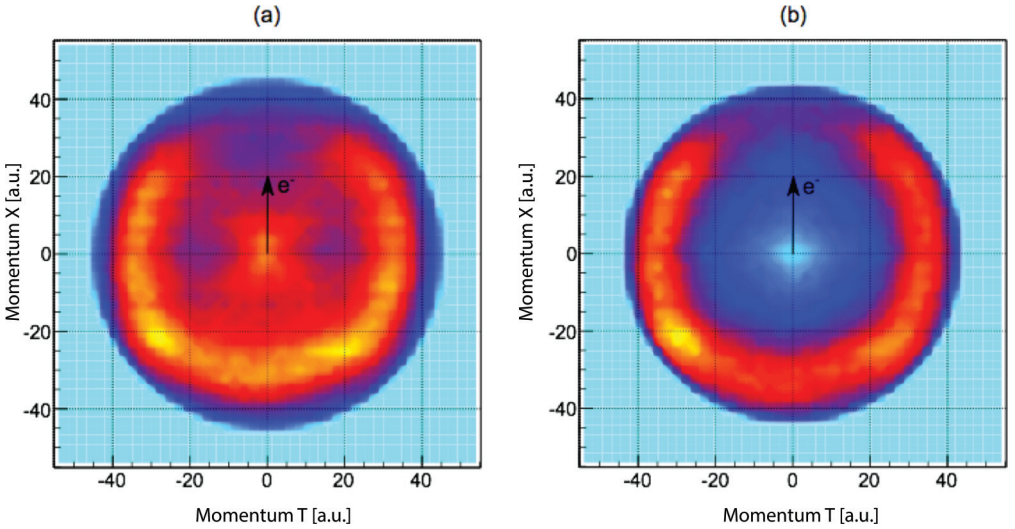

FIG. 2. (Color online) Linear-scale density plots of the O^- dissociation fragment momenta at 8.2 eV. (a) Slice of the O^- dissociation fragment momentum-space in the XT plane. No solid angle weighting has been applied. (b) Slice of the O^- dissociation fragment momentum-space in the XT plane. Solid angle weighting has been applied. The initial incoming electron direction is up. See the text for an explanation of the solid angle weighting.

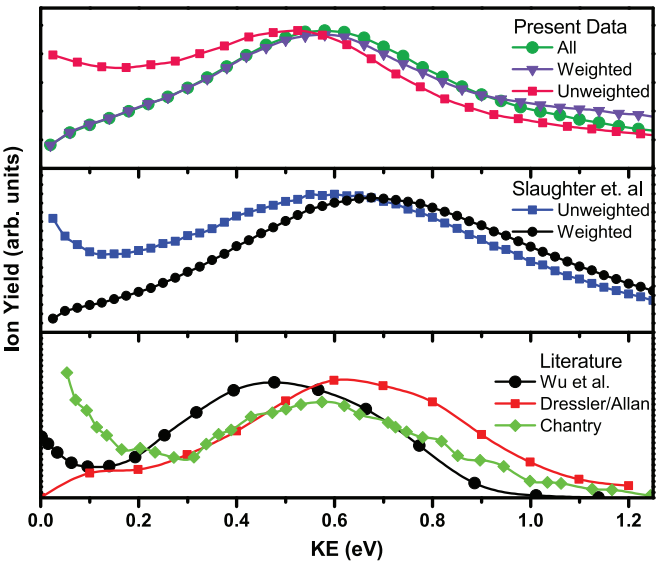

FIG. 3. (Color online) Kinetic energy distributions for O^- fragments from previous and present work. Top panel: Present O^- kinetic energy release data at 8.2 eV. The weighted data (filled triangles) shows a diminished contribution from low energy anions compared to the unweighted data (filled squares). The data labeled "All" (filled circles) include data over the full 4π range. This matches the weighted data supporting the solid angle weighting scheme. Middle panel: Data from Slaughter *et al.* [14] (filled squares) at 8.7 eV and the same data with our solid angle weighting applied (filled circles). Bottom panel: Data from Wu *et al.* [15] (filled circles), Dressler and Allan [8] (filled squares), and Chantry (filled diamonds).

polar angles for simplicity. A thin flat slice would include the entire contribution from the low kinetic energy component and only include a small fraction of ions having kinetic energy that is nonzero. If, instead of a thin flat slice, we confine the momentum to a solid angular range that is symmetrical in the detector plane, the ion yields at different energies will be comparable.

Complementary velocity slice imaging techniques [15] collect ion data for a sufficiently narrow time window in the center of the time-of-flight distribution to allow a 2D projection of the 3D ion distribution. The result is typically comparable to the flat slice of Fig. 2(a) that, as we have shown, exaggerates the yield of ions having low kinetic energy. Alternatively, Slaughter *et al.* [14] projected the full 3D momentum image onto a 2D plane to show the planar momentum distribution, which also exaggerates the small momentum contribution. The O^- momentum data of Slaughter *et al.* (Fig. 2 of Ref. [1]), when weighted in the same manner as the present data, are consistent with the results in Fig. 2(b).

Figure 3 shows various ion yields as a function of kinetic energy from the present experiment and previous work. The kinetic energy curve in our experiment is obtained by integrating the ejection angle of the O^- fragment and plotting the yield as a function of kinetic energy,

$$E_{\text{kin}} = \frac{p^2}{2m}, \tag{1}$$

where p is the absolute momentum and m is the mass of O^-.

In the top pane of Fig. 3 we illustrate the effect of solid-angle weighting and justify its use in interpreting the observed data. Since we have measured the complete 3D momentum of O^- fragments without slicing planes, we can obtain a kinetic energy release distribution over a full 4π solid angle. This result is plotted as "All" in the top pane of Fig. 3. If we then take a momentum-space slice and weight for solid angle as previously described, we obtain the data labeled "Weighted" in the top pane of Fig. 3. Alternatively, if we integrate over the momentum-space slice without weighting for solid angle we obtain the data labeled "Unweighted." Clearly, the weighted slice best represents the overall kinetic energy distribution of fragments from the unbiased 4π data.

The middle and bottom panes of Fig. 3 show that the unweighted data from our experiment is in agreement with each set of previously published data, except the data of Dressler and Allan [8]. The kinetic energy release data of Wu I. [15] is from an unweighted flat slice from a phosphor screen image, similar to Fig. 2(a). Slaughter *et al.* [14] used a coordinate transformation to plot the momentum's transverse and longitudinal components (with respect to the electron momentum vector) which also results in a momentum-space image similar to Fig. 2(a). When the data of Slaughter *et al.* are weighted for solid angle, their results match our weighted data, as shown in the middle pane of Fig. 3. This suggests that the low kinetic energy contribution, which is linked to considerable CO fragment vibrational excitation, is not as pronounced as previously suggested by earlier work and that this can serve as guidance for theoretical models of the potential energy surfaces and associated dissociation dynamics of CO_2 upon attachment.

Our measured angular distribution of O^- anions from dissociative attachment to CO_2 are shown in Fig. 4 along

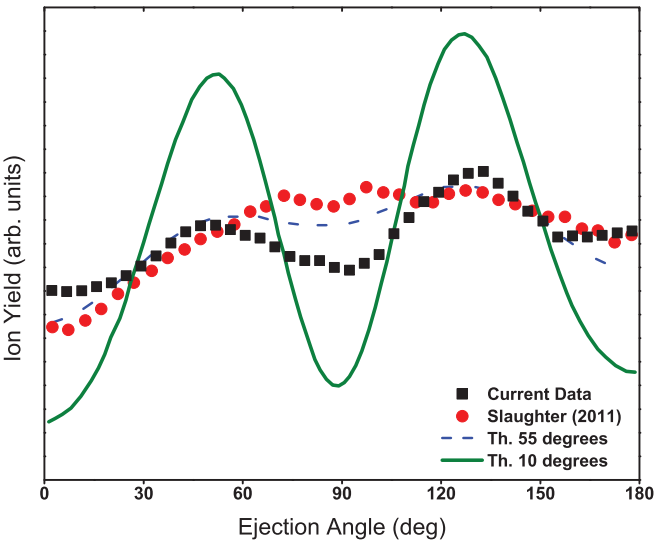

FIG. 4. (Color online) Angular distribution of O^- dissociation fragments from the present experiment for 8.2-eV electrons (filled squares), and experimental data from Slaughter *et al.* [14] (filled diamonds) at 8.2 eV. The theoretical angular distribution assuming axial recoil and convoluted by a Gaussian distribution of 10° FWHM (solid curve) and 55° FWHM simulating nonaxial recoil bending dynamics (dashed curve) are taken from Slaughter *et al.* [14].

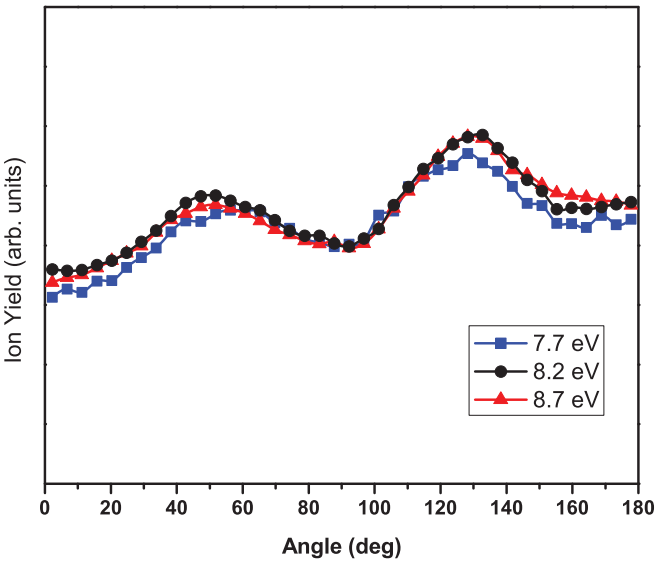

FIG. 5. (Color online) Angular distribution of O^- dissociation fragments for three electron impact energies, 7.7 eV (filled squares), 8.2 eV (filled circles), and 8.7 eV (filled triangles). The distributions show no significant dependence on energy in the observed range.

with theoretical calculations and measurement from Slaughter *et al*. The two theory curves show the angular distribution assuming root-mean-square values of the nuclei positions under asymmetric stretch and bending modes. These theoretical angular distributions were then convolved with Gaussian distributions of 10° and 55° FWHM to simulate the estimated angular resolution of the experiment and bending dynamics, respectively. As with the experimental data of Slaughter *et al*. [14], our current measurement clearly shows better agreement with the 55° convolved theory curve, implying a strong nonaxial recoil effect due to the bend and stretch contributions to the dissociation dynamics. As can be seen in Fig. 4, our experiment seems to have slightly better angular resolution as compared to Slaughter *et al*. The present experimental angular resolution is estimated to be better than 10° FWHM, an improvement over earlier experiments due to the use of a well localized target from a supersonic gas jet, as compared to an effusive target.

The previously reported measurements by Wu *et al*. [15] utilized the formalism of O'Malley and Taylor [20] to express the O^- angular dependence as a function of spherical harmonics corresponding to a splitting of the rovibrational state upon excitation of the vibrational bending mode v_2. Under conditions where the axial recoil approximation is valid [20], a description of the electron attachment process can be accurately determined with such a treatment. Slaughter *et al*. [14] employed an *ab initio* theoretical approach to determine the entrance amplitude and predict the ion angular distribution for the axial recoil case, which was found to differ remarkably from their experimental data and is confirmed by our experiment, suggesting a departure from axial recoil conditions.

The previous measurements by Wu *et al*. also indicate a varying angular distribution at electron energies on either side of the DEA resonance peak at 8.2 eV, suggesting the involvement of different, closely lying states. In Fig. 5 we show our measured angular distributions of O^- at the 8.2-eV DEA resonance peak as well as the same 7.7- and 8.7-eV energy points measured by Wu *et al*. The angular distributions in Fig. 5 indicate that the distributions are not visibly affected by the varying impact energy across the resonance. This is contrary to results presented by Wu *et al*. in which the angular distribution varied significantly with the electron energy.

IV. CONCLUSIONS

We have used a momentum imaging apparatus to determine the kinetic energy distribution and angular dependence of O^- formation from dissociative attachment to CO_2 around the 8-eV resonance. The kinetic energy distributions obtained by weighting the ion yield contributions for solid angle are qualitatively different from that obtained in previous works. The outcome of which has implications for the modeling of potential energy surfaces and associated dynamics on this well researched system, including at the lower energy resonance of 4 eV. The measured angular distributions confirm the nonaxial recoil bending dynamics observed by Slaughter *et al*. We also show that, contrary to the previous measurements by Wu *et al*., there is no significant change in the O^- angular distribution as a function of energy across the 8.2-eV DEA resonance.

ACKNOWLEDGMENTS

The authors acknowledge support from T. N. Rescigno, D. J. Haxton, A. E. Orel, and C. W. McCurdy (Lawrence Berkeley National Laboratory) for discussions and the included calculations.

[1] A. Stamatovic and G. Schulz, Rev. Sci. Instrum. **41**, 423 (1970).
[2] D. Rapp and D. D. Briglia, J. Chem. Phys. **43**, 1480 (1965).
[3] R. Abouaf, R. Paineau, and F. Fiquet-Fayard, J. Phys. B **9**, 303 (2001).
[4] M. Tronc, L. Malegat, and R. Azria, Chem. Phys. Lett. **92**, 551 (1982).
[5] S. K. Srivastava and O. J. Orient, Phys. Rev. A **27**, 1209 (1983).
[6] C. R. Claydon, G. A. Segal, and H. S. Taylor, J. Chem. Phys. **52**, 3387 (1970).
[7] P. J. Chantry, J. Chem. Phys. **57**, 3180 (1972).
[8] R. Dressler and M. Allan, Chem. Phys. **92**, 449 (1985).
[9] H. Adaniya, D. S. Slaughter, T. Osipov, T. Weber, and A. Belkacem, Rev. Sci. Instrum. **83**, 023106 (2012).
[10] D. Nandi, V. S. Prabhudesai, E. Krishnakumar, and A. Chatterjee, Rev. Sci. Instrum. **76**, 053107 (2005).
[11] B. Wu, L. Xia, H. K. Li, X. J. Zeng, and S. X. Tian, Rev. Sci. Instrum. **83**, 013108 (2012).
[12] M. Sizun and S. Goursaud, J. Chem. Phys. **71**, 4042 (1979).
[13] M. A. Huels, L. Parenteau, P. Cloutier, and L. Sanche, J. Chem. Phys. **103**, 6775 (1995).

[14] D. S. Slaughter, H. Adaniya, T. N. Rescigno, D. J. Haxton, A. E. Orel, C. W. McCurdy, and A. Belkacem, J. Phys. B **44**, 205203 (2012).
[15] B. Wu, L. Xia, Y. F. Wang, H. K. Li, X. J. Zeng, and S. X. Tian, Phys. Rev. A **85**, 052709 (2012).
[16] A. Moradmand, J. B. Williams, A. Landers, and M. Fogle, Rev. Sci. Instrum. **84**, 033104 (2013).
[17] R. Dörner, V. Mergel, O. Jagutzki, L. Spielberger, J. Ullrich, R. Moshammer, and H. Schmidt-Böcking, Phys. Rep. **330**, 95 (2000).
[18] Roentdek Handels GmbH, COBOLDPC 2008 (2008–2012).
[19] F. Rademakers, ROOT v2.24/05 (1994–2012).
[20] T. F. O'Malley and H. S. Taylor, Phys. Rev. **176**, 207 (1968).